

# High star formation activity in the central region of a distant cluster at $z=1.46$

Masao Hayashi,<sup>1\*</sup> Tadayuki Kodama,<sup>2</sup> Yusei Koyama,<sup>1</sup> Ichi Tanaka,<sup>3</sup>  
 Kazuhiro Shimasaku,<sup>1,4</sup> and Sadanori Okamura<sup>1,4</sup>

<sup>1</sup>*Department of Astronomy, Graduate School of Science, University of Tokyo, Tokyo 113-0033, Japan*

<sup>2</sup>*Optical and Infrared Astronomy Division, National Astronomical Observatory, Mitaka, Tokyo 181-8588, Japan*

<sup>3</sup>*Subaru Telescope, National Astronomical Observatory of Japan, 650 North A'ohoku Place, Hilo, HI 96720, USA*

<sup>4</sup>*Research Center for the Early Universe, Graduate School of Science, University of Tokyo, Tokyo 113-0033, Japan*

Accepted 2009 November 10. Received 2009 September 25; in original form 2009 August 2

## ABSTRACT

We present an unbiased deep [O II] emission survey of a cluster XMMXCS J2215.9-1738 at  $z = 1.46$ , the most distant cluster to date with a detection of extended X-ray emission. With wide-field optical and near-infrared cameras (Suprime-Cam and MOIRCS, respectively) on Subaru telescope, we performed deep imaging with a narrow-band filter *NB912* ( $\lambda_c = 9139\text{\AA}$ ,  $\Delta\lambda = 134\text{\AA}$ ) as well as broad-band filters (*B*, *z'*, *J* and *K<sub>s</sub>*). From the photometric catalogues, we have identified 44 [O II] emitters in the cluster central region of  $6' \times 6'$  down to a dust-free star formation rate of  $2.6 M_{\odot}/\text{yr}$  ( $3\sigma$ ). Interestingly, it is found that there are many [O II] emitters even in the central high density region. In fact, the fraction of [O II] emitters to the cluster members as well as their star formation rates and equivalent widths stay almost constant with decreasing cluster-centric distance up to the cluster core. Unlike clusters at lower redshifts ( $z \lesssim 1$ ) where star formation activity is mostly quenched in their central regions, this higher redshift 2215 cluster shows its high star formation activity even at its centre, suggesting that we are beginning to enter the formation epoch of some galaxies in the cluster core eventually. Moreover, we find a deficit of galaxies on the red sequence at magnitudes fainter than  $\sim M^* + 0.5$  on the colour-magnitude diagram. This break magnitude is brighter than that of lower redshift clusters, and it is likely that we are seeing the formation phase of more massive red galaxies in the cluster core at  $z \sim 1$ . These results may indicate inside-out and down-sizing propagation of star formation activity in the course of cluster evolution.

**Key words:** galaxies: clusters: general – galaxies: clusters: individual: XMMXCS J2215.9-1738 – galaxies: evolution.

## 1 INTRODUCTION

Galaxy formation and evolution is strongly dependent on environment and on galaxy mass (e.g., Dressler et al. 1997; Tanaka et al. 2005; Cooper et al. 2006; Tasca et al. 2009). Galaxies in high density regions are systematically older than those in lower density regions, and massive galaxies are on average older than lower mass galaxies in stellar ages. It seems that massive galaxies in the high density regions form first and galaxy formation activity is propagated to lower density regions and to lower-mass galaxies with time.

Such dependence on environment and mass can be understood by intrinsic effects and extrinsic effects. Intrinsic ef-

fects are those determined by the initial condition of galaxy formation and extrinsic effects are those in effect during the evolution of galaxies after formation.

The environmental dependence can be partly understood by the intrinsic effect called “galaxy formation bias” (e.g., Cen & Ostriker 1993) where high density regions should have started off from the largest initial density fluctuations that collapse first in the universe, and galaxy formation takes place earliest in such regions and subsequent evolution is prompted. In lower density regions, however, galaxy formation is delayed and time scales of star formation and mass assembly are longer. Likewise, the mass dependence of galaxy formation called “down-sizing” (e.g., Cowie et al. 1996; Kodama et al. 2004a) may be partly understood by the scaled-down version of the bias on galactic scale, where more

\* E-mail: hayashi@astron.s.u-tokyo.ac.jp

massive galaxies today correspond to higher initial density fluctuations on galactic scale and their formation such as star formation and assembly of building blocks take place earlier than less massive galaxies.

Galaxies are also subject to external effects from their surrounding environments, such as galaxy-galaxy interactions/mergers and ram-pressure stripping in dense environments (e.g., Abadi, Moore & Bower 1999; Quilis, Moore & Bower 2000). Such interactions may enhance and/or quench the star formation activity in galaxies preferentially in high density regions, which would therefore result in conspicuous dependence of galaxy properties on environments.

However, the relative importance of the intrinsic effects and the extrinsic effects is almost totally unknown yet. One of the most effective methods to verify the existence of the intrinsic effects is to go back in time and directly see the galaxies in the distant universe. By doing so, we may eventually reach the epoch when galaxies are forming rapidly in the biased cluster core, while galaxies are not yet formed or only slowly forming in lower density regions. Also, as we go back in time, host galaxies of star formation would be shifted to higher mass systems and we may eventually see the active star formation in action in massive galaxies in the cluster core.

In the low redshift universe, star formation activity is a monotonically decreasing function of local density. However, we have not yet known the dependence of star formation activity on environments at high redshifts in detail. According to recent studies, it seems that star formation is in fact biased at high density region at high redshifts. Elbaz et al. (2007) reported for the first time in the GOODS North/South surveys that at  $z \sim 1$  the galaxies at denser environment tend to have higher star formation rates (SFRs), in contrast to the local Universe. Cooper et al. (2008) and Ideue et al. (2009) also showed similar trends for [O II] emitters at  $z \sim 1$  in DEEP2 and COSMOS surveys, respectively. At a slightly lower redshift,  $z = 0.81$ , based on the mid-infrared observation of the RX J1716.4+6708 cluster, Koyama et al. (2008) reported that the star formation activity is probably enhanced in the medium density region, such as cluster outskirts or galaxy groups, rather than in the highest density region. Poggianti et al. (2008) also suggested that SFRs of galaxies may have a peak at intermediate densities at  $z=0.4-0.8$  based on the EDisCS survey. These observational findings may imply that the environment that hosts active star formation is shifted towards denser regions at higher redshifts.

On the other hand, it is well-known as the ‘‘Butcher-Oemler (B-O) effect’’ that more distant clusters show higher fraction of blue galaxies up to  $z \sim 0.5$ , suggesting the enhancement of star formation activity in higher- $z$  clusters (e.g., Butcher & Oemler 1978, 1984; Margoniner et al. 2001). However, the fraction of blue galaxies decreases with cluster centric radius, and red galaxies still dominate in the core regions at  $z \sim 0.5$  (Kodama & Bower 2001; Ellingson et al. 2001). Such studies of the B-O effect in clusters have been extended up to  $z \sim 1$ . Postman, Lubin & Oke (2001) found that the fraction of active galaxies in the central regions of clusters is higher at  $z \sim 0.7-0.9$  compared to  $z \sim 0.2-0.5$ . However, Nakata et al. (2005) suggested that the fraction of galaxies with strong [O II] emission in the cluster cores at  $z < 1.0$  is not significantly dependent on redshift. It thus

seems that we have not yet reached a bursting phase of massive galaxy formation in cluster cores even at  $z \sim 1$ , although the global activity of star formation within clusters is already enhanced.

In this paper, we present an [O II] emitter survey of the XMMXCS J2215.9-1738 cluster (hereafter 2215 cluster) with a narrow-band filter *NB912* on Suprime-Cam (Figure 1), and discuss spatial distribution of star formation activity (see also Koyama et al. 2010, which presents our H  $\alpha$  emitter survey of the RX J1716.4+6708 cluster at  $z = 0.81$ ). The 2215 cluster is the most distant cluster to date at  $z=1.46$  with a detection of extended X-ray emission (Stanford et al. 2006). Hilton et al. (2007, 2009) have confirmed dozens of the cluster members by spectroscopy, and found that velocity dispersion of the member galaxies is  $\sigma = 580 \pm 140$  [km s $^{-1}$ ]. With the *NB912* filter, we can survey [O II] emissions from the galaxies with the line-of-sight velocities between  $-2794 < \Delta V_{\text{los}} [\text{km s}^{-1}] < 1598$  with respect to the velocity centre of the cluster. Our *NB912* filter thus perfectly matches this cluster, and should be able to detect all the [O II] emission lines from the cluster members to a certain flux limit without introducing any bias (Figure 1). Therefore, our survey is unique, and the 2215 cluster is an ideal target for us to investigate the environmental dependence of star formation activity over a wide range in environment at this high redshift.

The X-ray luminosity and inter-cluster medium temperature for the 2215 cluster are  $L_X = 4.4_{-0.6}^{+0.8} \times 10^{44}$  [erg s $^{-1}$ ], and  $kT = 7.4_{-1.8}^{+2.6}$  [keV], respectively (Stanford et al. 2006). The luminosity is fainter than what is expected from the temperature compared to the local  $L_X - T$  relation. Hilton et al. (2007) thus point out that this cluster may experience a merger within the last few Gyr. It is also found that colour-magnitude diagram in this cluster shows red sequence (Stanford et al. 2006; Hilton et al. 2009). Hilton et al. (2009) investigated the morphologies of bright member galaxies, and found that about 60% of members are E or S0 galaxies. Even at  $z = 1.46$ , cluster core is already dominated by early-type galaxies, as far as morphology is concerned.

The structure of this paper is as follows. The observations and data reduction are described in § 2. In § 3, we describe how we select the [O II] emitters associated to the cluster at  $z = 1.46$  from the photometric catalogues. We show the spatial distribution, SFRs, and equivalent widths of the [O II] emitters, and investigate the star forming activity in the 2215 cluster in §4. We also discuss the deficit of faint red galaxies and its evolution. A summary is given in §5. Throughout this paper, magnitudes are in the AB system, and we adopt cosmological parameters of  $h = 0.7$ ,  $\Omega_{m0} = 0.3$  and  $\Omega_{\Lambda0} = 0.7$ . Vega magnitudes in  $J$  and  $K_s$ , if preferred, can be obtained from our AB magnitudes using the relations:  $J(\text{Vega})=J(\text{AB})-0.92$  and  $K_s(\text{Vega})=K_s(\text{AB})-1.80$ .

## 2 OBSERVATIONS AND DATA REDUCTION

We have obtained optical ( $B$ ,  $z'$ , and *NB912*) and near-infrared ( $J$  and  $K_s$ ) images of the 2215 cluster for selection of [O II] emitters and member galaxies in the cluster. The observed data are summarized in Table 1.

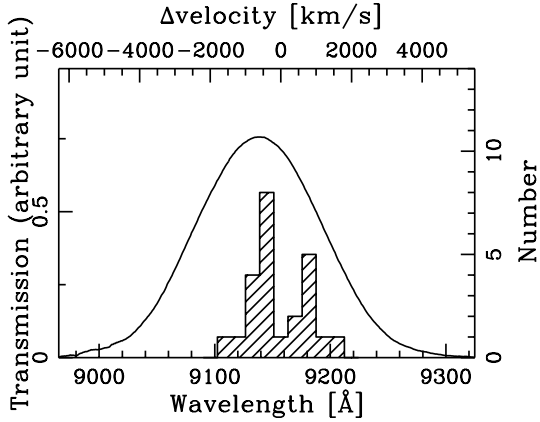


**Figure 1.** A transmission curve of the *NB912* filter ( $\lambda_c=9139\text{\AA}$ ,  $\Delta\lambda=134\text{\AA}$ ). Upper x-axis shows peculiar velocity with respect to the velocity centre of the cluster at  $z = 1.46$ . The histograms show the velocity distribution of the spectroscopically confirmed member galaxies of the 2215 cluster (Hilton et al. 2009).

## 2.1 Optical data

The optical imaging was conducted using Subaru/Suprime-Cam with fully-depleted back-illuminated CCDs (Miyazaki et al. 2002) on 2008 July 30 and 31. Suprime-Cam has a wide field-of-view (FoV) of  $34\times 27$  arcmin<sup>2</sup>, and the quantum efficiency of CCDs in red wavelengths, such as  $z'$ -band, is considerably improved by replacement with fully-depleted-type CCDs in the S08A semester (Kamata et al. 2008). We have obtained two broad-band data of *B* and  $z'$ , and a narrow-band data of *NB912* (Figure 1;  $\lambda_c=9139\text{\AA}$ ,  $\Delta\lambda=134\text{\AA}$ ). The individual exposure times of a frame in *B*,  $z'$  and *NB912* were 20, 5, and 20 minutes, and the total integration times were 160, 90, and 360 minutes, respectively. The weather was fine during the two nights of our observing run, and the sky conditions were photometric all the time, except for the first half of the night on July 30. The seeing sizes were 0.6–0.9 arcsec in *B*, 0.8–1.0 arcsec in  $z'$ , and a wide range of 0.6–2.0 arcsec in *NB912*. It is noted that the *NB912* data with bad seeing were taken under marginal condition on July 30.

The data reduction is conducted with a data reduction package for Suprime-Cam (SDFRED ver.1.4: Yagi et al. 2002; Ouchi et al. 2004). However, since the currently distributed package is not applicable to the data obtained after the upgrade of CCDs, we have modified the software accordingly. The data in each passband are reduced following a standard procedure: We first rejected some frames with bad seeing or low signal-to-noise ratio due to high sky background. A self-flat image is then created from all the object frames after bias subtraction, and we use it for flat fielding. A sky is subtracted and an instrumental distortion is then corrected for on each object frame. Point spread functions (PSFs) in all images are matched to 1.09 arcsec, which is the worst seeing size of the *NB912* data. Finally, after masking satellite trails and bad quality regions, the flux calibrated images are mosaiced and co-added to make a final image (Figure 2). The net integration times in *B*,  $z'$ , and *NB912* are 140, 80, and 260 minutes, and the seeing size in the final images is 1.09 arcsec. The zero-point magnitudes are determined using spectrophotometric standard stars (Oke 1990)

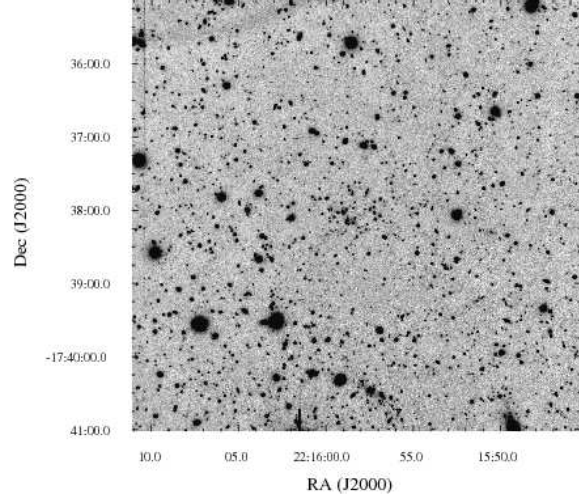


**Figure 2.** The co-added narrow-band (*NB912*) image of XMMXCS J2215.9-1738 cluster taken with Suprime-Cam. North is up, and east is left. The field of view is limited to a central  $\sim 6\times 6$  arcmin<sup>2</sup> region, corresponding to a  $\sim 3\times 3$  Mpc<sup>2</sup> area, which overlaps with our NIR imaging with MOIRCS. In this paper, we focus only on this relatively inner region of the cluster.

for  $z'$  and *NB912*, and a Landolt (1992) photometric standard star for *B*, respectively. The  $3\sigma$  limiting magnitudes are 27.6, 25.8, and 25.8 in *B*,  $z'$  and *NB912*, respectively.

In this FoV, there are several bright stars that are saturated especially in *B*. These saturated regions are masked, and are not used in the following analyses.

## 2.2 Near-infrared data

The near-infrared (NIR) imaging was carried out with Subaru/MOIRCS (Ichikawa et al. 2006; Suzuki et al. 2008) on 2008 June 29 and 30, and we have obtained images of a central  $6\times 6$  arcmin<sup>2</sup> area of the 2215 cluster in two broadbands, *J* and  $K_s$ . MOIRCS has a FoV of  $7\times 4$  arcmin<sup>2</sup>, which consists of two chips with a FoV of  $4\times 4$  arcmin<sup>2</sup> each. Unfortunately, at the time of our observation, chip 1 was of an engineering grade, and had a lower quantum efficiency than chip 2 of a scientific grade. We therefore observed at each position with two position angles of 0 and 180 degrees. Therefore, four pointings were required in total to cover the entire  $6' \times 6'$  region with the chip 2. The exposure times of a frame in *J* and  $K_s$  are 120 and 40 seconds, respectively, and three frames were co-added at each dither point in  $K_s$ . The total integration times in *J* and  $K_s$  have a range of 32.5–67.5 and 18–30 minutes, respectively, depending on the pointing. The sky conditions were photometric during the two nights of our observing run. The seeing sizes were 0.4–0.7 arcsec in *J* and 0.4–0.8 arcsec in  $K_s$ .

The data reduction is conducted with a data reduction package for MOIRCS (MCSRED ver.20081023: Tanaka et al. in preparation). The data are reduced following a standard procedure: A flat-fielding is done using a self-flat image created from the object frames. A sky is subtracted and instrumental distortion is then corrected for on each image. In the MOIRCS frames, especially those taken by chip 2, strong fringe pattern are sometimes seen, which are removed

**Table 1.** Summary of the observed data. The limiting magnitudes are measured with a  $2''$  diameter  $\phi$ . Depth of the NIR data depends on the pointing due to different integration times. The seeing sizes in all the co-added images are matched to 1.09 arcsec. In this paper, we will concentrate only on the central  $6 \times 6$  arcmin<sup>2</sup> region where the NIR data co-exist.

filter	effective FoV (arcmin <sup>2</sup> )	net integration (minutes)	limiting mag. ( $3\sigma$ )
<i>B</i>	32×23	140	27.6
<i>z'</i>	32×23	80	25.8
<i>NB912</i>	32×23	260	25.8
<i>J</i>	6×6	32.5 – 67.5	23.8 – 24.6
<i>K<sub>s</sub></i>	6×6	18 – 30	23.1 – 23.6

from the images. We masked some regions with low signal-to-noise ratio such as the edges of the frames, matched the PSF sizes, and mosaiced and co-added to make the final images. The seeing sizes in *J* and *K<sub>s</sub>* images are degraded to 1.09 arcsec to match the optical images. The zero-point magnitudes are determined using a faint standard star in Leggett (2006) that we observed during our run. The  $3\sigma$  limiting magnitudes are 23.8–24.6, and 23.1–23.6 in *J* and *K<sub>s</sub>*, respectively.

In what follows, we focus only on the central region ( $33.8$  arcmin<sup>2</sup>) of the 2215 cluster (Figure 2) where both NIR and optical data exist, because the NIR data are crucial to identify member galaxies of the cluster.

### 3 SELECTION OF CLUSTER MEMBERS AND [O II] EMITTERS

#### 3.1 Catalogues

##### 3.1.1 *NB912*-detected catalogue

We use SExtractor (ver. 2.5.0: Bertin & Arnouts 1996) for source detection and photometry. Objects are detected in *NB912*, and their photometries in all images are carried out at the same positions as on the *NB912* image using the double-image mode of SExtractor. All images are geometrically matched to the *NB912* data. We then select 1575 objects brighter than  $5\sigma$  limiting magnitude in *NB912*, where objects in masked regions are excluded. Color indices are derived within a  $2''$ -diameter aperture, and MAG\_AUTO magnitudes are used as total magnitudes.

Stars and galaxies are separated based on their  $B - z'$  and  $z' - K_s$  colours according to the same procedure as in Hayashi et al. (2007) (see also Daddi et al. 2004, Kong et al. 2006). Among 1575 objects, 158 are classified as stars, and the remaining 1417 are classified as galaxies. Using the stellar sample, we check the zero points of magnitudes in all the optical and NIR images by comparing stellar colours with those of stellar spectrophotometric atlas of Gunn & Stryker (1983). No correction is applied for all the bands since stellar colours are in good agreement with those of the stellar atlas, except for the  $z'$ -band in which we shifted the zero-point by only 0.05 magnitude.

Next, we compare differences between aperture magnitude and total magnitude in all bands for galaxy sample,

and find that aperture magnitudes are a little fainter systematically than total magnitudes in only  $z'$ -band. Therefore, aperture correction of 0.05 magnitude is applied for aperture magnitudes in  $z'$  so that an aperture contains the same fraction to total in all bands. In addition, magnitude is corrected for galactic absorption,  $A(B)=0.10$ ,  $A(z')=0.04$ ,  $A(NB912)=0.04$ ,  $A(J)=0.02$ , and  $A(K_s)=0.01$ , which are estimated using extinction law of Cardelli, Clayton & Mathis (1989) on the assumption of  $R_V=3.1$  and  $E(B - V)=0.025$  at the central coordinates of the 2215 cluster according to Schlegel, Finkbeiner & Davis (1998).

Magnitude errors are estimated from  $1\sigma$  sky noise taking account of the difference in depth at each object position due to slightly different exposure times and sensitivities.

##### 3.1.2 *K<sub>s</sub>*-detected catalogue

We also create a *K<sub>s</sub>*-detected catalogue using the same procedure as we used for the *NB912*-detected catalogue, except that *K<sub>s</sub>*-band image is used instead for source detection. We then select 1198 objects (115 stars and 1083 galaxies) brighter than  $K_s=23.0$ , which corresponds to  $\sim 5\sigma$  limiting magnitude in most of the regions and  $\sim 3\sigma$  in the shallowest region.

The *K<sub>s</sub>*-detected catalogue is used only in §4.3 for discussion based on the  $z' - K_s$  vs.  $K_s$  colour-magnitude relation of the cluster members. For the rest of the paper, the *NB912*-detected catalogue is used unless otherwise mentioned.

#### 3.2 Cluster member candidates

It would be ideal of course to use spectroscopic redshifts to determine membership of individual galaxies. The lack of such complete spectroscopic data, however, forces us to estimate membership based on our existing photometries. In this paper, we use a  $B - z'$  vs.  $z' - K_s$  colour-colour diagram, in analogy to the BzK selection of galaxies (Daddi et al. 2004). We note that our scheme is very simple and easily reproducible, unlike commonly used photometric redshifts based on spectral fitting to some model or empirical templates. We apply the following colour criteria,

$$(z' - K_s) > (B - z') - 0.46 \cup (z' - K_s) > 2.2, \quad (1)$$

in order to remove the foreground and background galaxies (red solid lines in Figure 3(a)). We modify the original BzK criteria (broken lines in Figure 3(a); Daddi et al. 2004) that has been designed to select both star-forming and passively evolving galaxies at  $1.4 \lesssim z \lesssim 2.5$ . Since the redshift under concern in this paper, namely the cluster redshift of 1.46, is close to the lowest edge of the applicable redshift range of the BzK selection, we loosen the original boundary of the BzK selection as indicated by solid lines in Figure 3(a) to increase the completeness of galaxies at  $z = 1.46$ . Consequently, it is also obvious that our criteria will select a large number of background galaxies up to  $z \sim 2.5$  which are contaminants for our use. However, for the narrow-band emitters in *NB912*, we just need to separate out the [O II] line emitters from other line emitters such as H $\alpha$  and [O III] in the foreground and background at some specific redshifts. These unwanted emitters are well separated on this diagram.

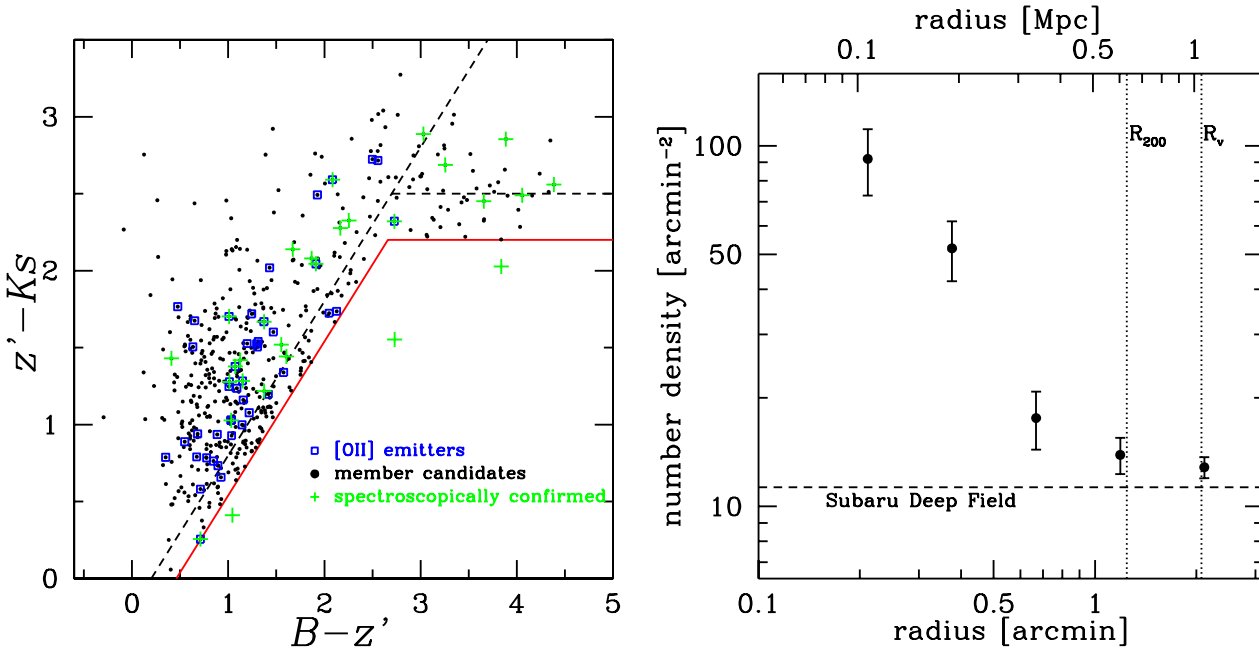


**Figure 3.** (a) Left panel: The colour-colour diagram of  $B - z'$  vs.  $z' - K_s$ . The red solid lines show our selection criteria for cluster member candidates, while the black broken lines indicate the original BzK selection criteria defined by Daddi et al. (2004). Blue open squares show 44 [O II] emitters in the 2215 cluster, black dots are cluster member candidates, and green crosses indicate spectroscopically confirmed cluster members in Hilton et al. (2007, 2009). (b) Right panel: The number density of cluster member candidates as a function of radius from the cluster centre. Error bars show Poisson errors. Vertical lines show the radii of  $R_{200} = 0.63\text{Mpc}$  and  $R_v = 1.05\text{Mpc}$ , respectively (Hilton et al. 2007). Horizontal line indicates the number density of Subaru Deep Field galaxies selected with the same criteria.

For the non-emitters, we will apply a statistical correction to the above defined cluster member candidates, using a blank field data in the Subaru Deep Field (see below).

We use the *NB912*-detected catalogue to select cluster member candidates. If an object is not detected at more than  $2\sigma$  above the noise level in each band, its magnitude is converted to the  $2\sigma$  limiting magnitude, so that the upper/lower limit of colour can be derived. For membership, we only pick out the galaxies that strictly meet our colour criteria (the principle of our selection is similar to that used in Hayashi et al. 2007). Since the colour selection based on the BzK diagram for objects without secure  $K_s$ -band detection is uncertain, we exclude those fainter than the  $2\sigma$  limiting magnitude in  $K_s$  in the membership determination. We select 486 cluster member candidates from the *NB912*-detected catalogue, among which 365 galaxies meet the original BzK criteria. The number density is 14.4 per  $\text{arcmin}^2$ .

In our colour-selected member candidates, there must be a significant contamination of foreground/background galaxies that are not associated to the 2215 cluster. We estimate a contribution of such field galaxies by applying the same criteria and limiting magnitudes to a part of the Subaru Deep Field (SDF) of a  $453 \text{ arcmin}^2$  area which has deep  $K$  imaging data as well (Motohara et al. 2008). The number density of the colour-selected galaxies is 11.3 per  $\text{arcmin}^2$ , which is in good agreement with the number density in the outer region of the cluster (Figure 3(b)). The excess over the field density can be regarded as a cluster component. This implies that our estimations of the number density of field contamination, thus that of cluster members, are reasonable.

Hilton et al. (2009) reported 64 cluster members within the radius of 1.5 arcmin in the 2215 cluster. Among them, 24 galaxies are identified by spectroscopy, and the others are selected by photometric redshifts. The spectroscopically confirmed members are also plotted in Figure 3(a). We find that  $\sim 90\%$  of members in Hilton et al. (2009) are contained in our member candidate sample, which assures our member selection. Although three confirmed members are missed out in our selection, such low-level incompleteness would not significantly affect our statistical discussions in this paper. We then use our sample to estimate the number of cluster members after subtracting the field contribution, and find that our estimation of  $\sim 79 \pm 15$  members is compatible with the number in Hilton et al. (2009). This fact also supports the validity of our criteria for selection of cluster members.

### 3.3 [O II] emitters

We select galaxies with flux excess in *NB912* compared to  $z'$  to search for [O II] emitters in the 2215 cluster. The [O II] line ( $\lambda_{\text{rest}}=3727\text{\AA}$ ) emitted by galaxies at  $z = 1.46$  is redshifted just into the *NB912* filter, while the  $z'$ -band samples averaged continuum flux underneath the line. This survey based on  $z' - \text{NB912}$  colours is therefore best suited to this 2215 cluster and is able to search for [O II] emissions from almost all the member galaxies of the cluster to a certain flux limit. The galaxies with colour excesses in  $z' - \text{NB912}$  larger than  $3\sigma$  and  $z' - \text{NB912} > 0.2$  are identified as the *NB912* emitters. (Figure 4). The  $3\sigma$  colour of  $z' - \text{NB912}$  is derived as follows;

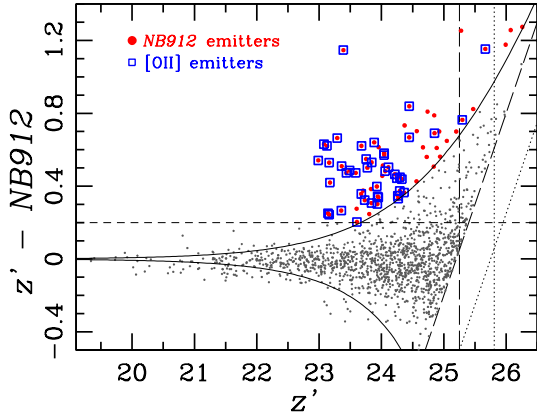


**Figure 4.** A colour-magnitude diagram of  $z'$  vs.  $z' - NB912$ . Solid lines show the  $3\sigma$  excesses of  $NB912$  over  $z'$ . Long-dashed and dotted lines show  $3\sigma$  and  $5\sigma$  limiting magnitudes, respectively. Short-dashed line shows  $z' - NB912 = 0.2$ . Gray dots show galaxies brighter than  $5\sigma$  in  $NB912$ . Red filled circles are 69  $NB912$  emitters, and blue open squares are 44 [O II] emitters in the 2215 cluster.

$$3\sigma_{z' - NB912} = -2.5 \log[1 \pm \sqrt{f_{3\sigma, z'}^2 + f_{3\sigma, NB912}^2 / f_{z'}^2}], \quad (2)$$

where  $f_{3\sigma}$  is  $3\sigma$  sky noise flux. The latter criterion is arbitrarily determined from the distribution of galaxy colours. However,  $z' - NB912$  colours of spectral templates of local galaxies (Coleman, Wu & Weedman 1980) redshifted over the range of  $z=0.0-3.0$  indicate that no galaxy would satisfy  $z' - NB912 > 0.2$  without having any emission line in  $NB912$ , suggesting we have no contamination from ordinary galaxies. The colour criteria correspond to [O II] flux  $\geq 1.4 \times 10^{-17}$  erg s $^{-1}$  cm $^{-2}$  and observed equivalent width  $\geq 35\text{\AA}$ , respectively. This means that our survey is sensitive to the [O II] emitters with a dust-free SFR larger than  $2.6 M_{\odot}\text{yr}^{-1}$  according to the the [O II] -SFR calibration in Kennicutt (1998).

In order to accurately measure the flux excess in  $NB912$  to  $z'$ , we may want to take into account the difference in continuum flux density, if any, between  $z'$  and  $NB912$  bands due to the slope of continuum spectrum. However, if we compare  $z' - NB912$  vs.  $z' - K_s$ , we found that there is no correlation between the two colours, and that  $z' - NB912$  colours are distributed around  $z' - NB912 = 0$  with a certain dispersion. We therefore conclude that the difference in continuum between  $z'$  and  $NB912$  is negligible. This is also supported by the fact that the difference in effective wavelengths between the two bands is small;  $\Delta\lambda \sim 100\text{\AA}$ . Therefore no correction for the colour term is made. After all, we select 69  $NB912$  emitters from 1417 galaxies in the  $NB912$ -detected sample. Out of the 69 emitters, 55 are detected in  $K_s$  at more than  $2\sigma$  levels.

Our  $NB912$  emitters could include galaxies with the following major strong lines such as  $H\alpha$  ( $\lambda_{\text{rest}}=6463\text{\AA}$ ,  $z=0.39$ ), [O III] ( $\lambda_{\text{rest}}=4959$  and  $5007\text{\AA}$ ,  $z=0.82-0.84$ ),  $H\beta$  ( $\lambda_{\text{rest}}=4861\text{\AA}$ ,  $z=0.88$ ), [O II] ( $\lambda_{\text{rest}}=3727\text{\AA}$ ,  $z=1.46$ ) and  $\text{Ly}\alpha$  ( $\lambda_{\text{rest}}=1216\text{\AA}$ ,  $z=6.51$ ). We then apply our selection criteria of cluster member candidates defined in §3.2 for the 55  $NB912$  emitters, of which 44 emitters are identified as [O II] emitters (Figure 4). Figure 5 shows a spatial distribution of those 44 [O II] emitters.

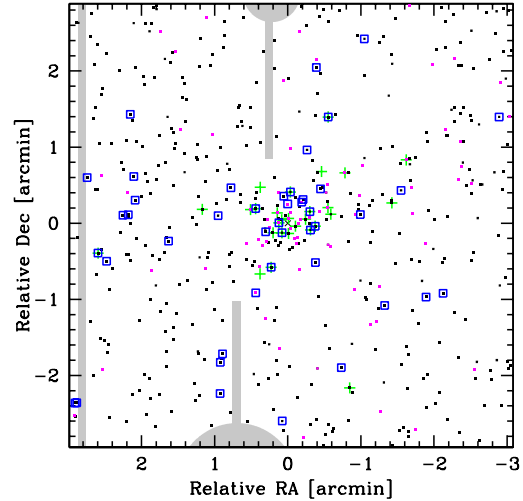


**Figure 5.** The celestial distribution of 44 [O II] emitters and cluster member candidates in the 2215 cluster. North is up, and east is to the left. Symbols are the same as those in Figure 3(a), except that magenta dots show red member candidates that satisfy  $z' - K_s > -0.088K_s + 4.26$  (lower broken line in Figure 9(a); see section 4.3). Gray areas indicate masked regions that we exclude from the analyses.

The empirical colour tracks between  $z = 0.0$  and  $1.5$  on the  $B - z'$  vs.  $z' - K_s$  diagram based on the spectral templates (Coleman et al. 1980) assure that most of the galaxies at  $z < 1.0$  cannot satisfy the colour selection of equation (1). Moreover, almost all the  $NB912$  emitters are detected in  $B$ -band at more than  $5\sigma$  confidence level, which would reject the possibility that the emission line is  $\text{Ly}\alpha$  at  $z = 6.51$ . Therefore, by applying the modified BzK selection, we can securely decontaminate other lines than [O II] at  $z=1.46$ .

We also use the samples of  $H\alpha$  ( $z = 0.4$ ), [O III] ( $z = 0.84$ ) and [O II] ( $z = 1.47$ ) emitters identified from the  $NB912$  emitters in the SDF (Ly et al. 2007) in order to verify our selection of [O II] emitters. Ly et al. (2007) separated  $H\alpha$  emitters based on  $R_c - i'$  vs.  $B - R_c$  colours, and then discriminated between [O III] and [O II] emitters based on  $i' - z'$  vs.  $R_c - i'$  colours, as well as some spectroscopic data where available. Although our method uses less colour information, i.e.  $B - z'$  and  $z' - K_s$  only, it is found that our criteria can still effectively separate [O II] lines from other possible lines.

We compare the number densities between our emitter samples and the SDF emitter samples (Ly et al. 2007) under the same selection criteria and limiting magnitude. We assume that the remaining 11  $NB912$  emitters other than [O II] in our sample are most likely to be strong  $H\alpha$  or [O III] lines, and compare its number density,  $0.33 \pm 0.10$  per arcmin $^2$ , with that of a combined sample of  $H\alpha$  and [O III] lines in the SDF,  $0.30 \pm 0.02$  per arcmin $^2$ . Since these emitters do not belong to the 2215 cluster at  $z = 1.46$ , this agreement in the number densities supports the validity of our line identification.

The number density of [O II] emitters in the cluster,  $1.3 \pm 0.2$  per arcmin $^2$ , is a factor of  $\sim 4$  larger than that of the SDF sample,  $0.34 \pm 0.02$  per arcmin $^2$ . Such excess are

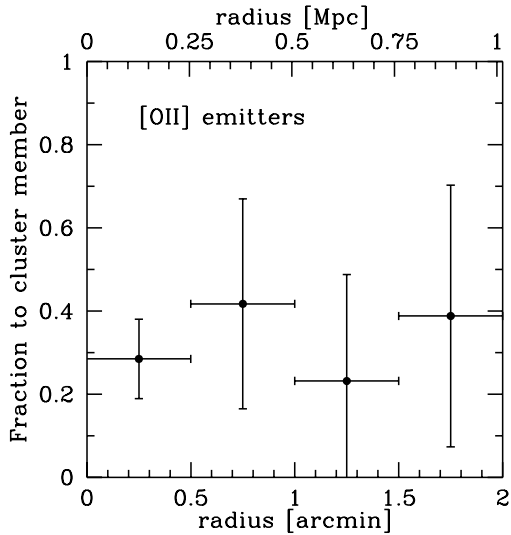


**Figure 6.** Fraction of [O II] emitters to the cluster members as a function of radius from a cluster centre. The contribution of field galaxies is statistically subtracted from our colour-selected cluster member candidates. The error-bars indicate the statistical errors associated to both [O II] emitters and the cluster members.

probably due to the existence of many [O II] emitters associated to the cluster at  $z=1.46$ . A cosmic variance due to our relatively small FoV ( $6' \times 6'$ ) of this study may contribute to the difference to some extent. We examine the number of [O II] emitters within randomly allocated  $6' \times 6'$  FoVs in the SDF, and find that the number of 44 [O II] emitters in the cluster is  $\sim 3.6\sigma$  excess than median field number density of [O II] emitters. This suggests that the difference is intrinsic and unlikely to be caused only by such cosmic variance.

## 4 RESULTS AND DISCUSSIONS

### 4.1 Star formation activity in a cluster core

Figure 5 shows that there are many [O II] emitters in the central region of the 2215 cluster. If we assume that [O II] lines are emitted from ionized gas in/around the star forming regions, it seems that the 2215 cluster is still actively forming stars even at its core region. This is not the case in lower- $z$  clusters where star forming activity is much lower in the central region. To be more quantitative, we estimate a fraction of [O II] emitters to cluster members as a function of cluster-centric distance in Figure 6. Here, the amount of remaining contamination from foreground/background galaxies are estimated from the SDF sample, and it is statistically subtracted from the colour-selected sample of cluster member candidates. Figure 6 suggests that the 2215 cluster maintains a high fraction of star forming galaxies in the central region,  $\sim 30\%$ , even at the most inner part within 0.25 Mpc in physical scale ( $1' = 0.51 \text{ Mpc}$  at  $z = 1.46$ ). This fraction is higher than the [O II] fraction in the cluster cores in Nakata et al. (2005), which is  $\lesssim 20\%$  at  $z < 1.0$ .

Lidman et al. (2008) recently reported a distribution of spectroscopic sample of [O II] emitters in a cluster XMMU J2235.3-2557 at  $z = 1.39$ , a similar redshift to that of the 2215 cluster. While there are no galaxies in the very

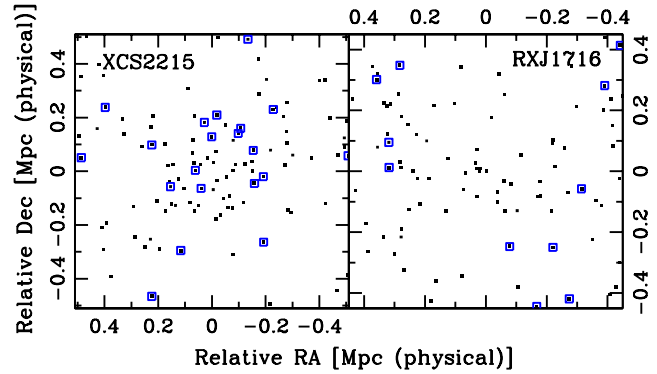


**Figure 7.** Close-up views of the central  $2' \times 2'$  regions for XCS2215 cluster at  $z = 1.46$  (left) and RXJ1716 cluster at  $z = 0.81$  (right). Blue open squares show [O II] emitters for 2215 cluster and  $H\alpha$  emitters for RXJ1716 cluster, respectively. Dots show cluster member candidates selected in §3.2 for the 2215 cluster, and member galaxies selected by photometric redshifts of  $\Delta z = 0.76 - 0.83$  for RXJ1716 cluster (Koyama et al. 2007), respectively. Both panels show the areas of similar physical scales (0.51 Mpc/arcmin at  $z = 1.46$  and 0.45 Mpc/arcmin at  $z = 0.81$ , respectively).

core within 90 kpc in radius that show star forming activity, [O II] lines are detected from more than half of galaxies near the centre. This result is similar to ours on the [O II] emitters in 2215 cluster at a similar (slightly higher) redshift of 1.46. It seems likely that distant X-ray detected clusters at  $z \gtrsim 1.4$  are actively forming new stars even in the central region within a few hundreds kpc in radius.

We have recently conducted a narrow-band  $H\alpha$  emitter survey for RX J1716.4+6708 cluster at  $z=0.81$  (Koyama et al. 2010 in preparation). This survey reveals quite a different situation where no  $H\alpha$  emitters are observed in the core region within a radius of 0.25 Mpc (Figure 7). A difference in spatial distribution of the emitters is very impressive. The  $H\alpha$  emitters in the 1716 cluster are selected with a combination of NB119 ( $\lambda_c = 11885\text{\AA}$ ,  $\Delta\lambda=141\text{\AA}$ ) and J filters on Subaru/MOIRCS. The  $H\alpha$  survey reached to the depth of a limiting line flux of  $\sim 4.1 \times 10^{-17} \text{ erg s}^{-1} \text{ cm}^{-2}$ , which corresponds to a dust-free SFR of  $\sim 1.0 M_{\odot} \text{ yr}^{-1}$ . The  $H\alpha$  survey for the 1716 cluster is, thus, more sensitive to star forming galaxies with slightly lower SFR than the [O II] survey for the 2215 cluster, presented in this paper.

Although the lines are different between the two clusters,  $H\alpha$  and [O II] lines, considering the fact that  $H\alpha$  line is much less affected by dust extinction than [O II] line, the intrinsic difference in spatial distribution of the emitters would be more significant. Furthermore, Koyama et al. (2010) find that the fraction of star forming galaxies decreases as one goes to denser region, which is different from what we see for the 2215 cluster. Similar trends are also found in lower redshift clusters at  $z=0.4-0.8$  (Kodama et al. 2004b; Poggianti et al. 2008). Koyama et al. (2008, 2010) have also unveiled the star forming activities hidden by dust in the 1716 cluster based on the mid-infrared imaging with AKARI. These studies conclude that star formation activity has already been quenched in the cluster core, while it comes to an peak in the medium density regions away from the cluster core.

These facts may imply that we find galaxy formation

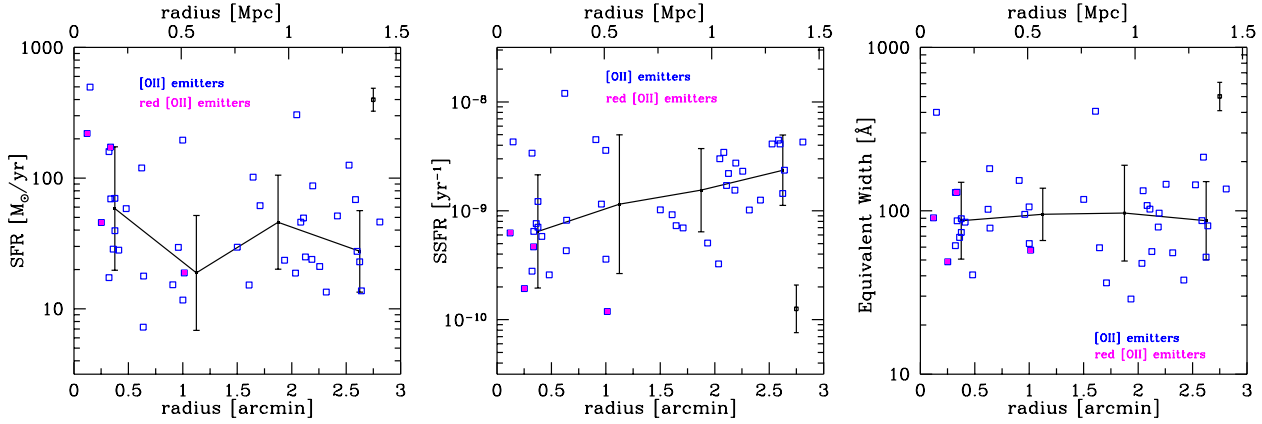


**Figure 8.** SFRs(left), specific SFRs (SSFRs) (middle) and observed equivalent widths (right) for [O II] emitters as a function of distance from the cluster centre. SFRs are derived and corrected for dust extinction using the relations in Moustakas et al. (2006) (see text). Stellar masses are estimated using the equation of Daddi et al. (2004). Equivalent widths are calculated with the equations (3) and (4). Blue open squares show 44 [O II] emitters, and 4 red [O II] emitters are marked by magenta filled square. Typical errors on each value are shown in the upper or the lower right corner on each panel. The errors on SFR and equivalent width are derived from magnitude errors in  $NB912$  and  $z'$ , and  $\sigma(\Delta \log(M_*)) = 0.20$  is applied to the error in stellar mass (see text). In each diagram, the solid line connects median values in four radius bins, and the errors contain both the typical error on each value and the standard deviation in each bin.

bias in the highest density region at  $z \sim 1.5$ . Recent studies also support the biased star formation in a relatively dense environment at  $z > 1$  (Elbaz et al. 2007; Cooper et al. 2008; Ideue et al. 2009). The difference of critical environments in star formation at various redshifts may suggest that galaxy formation bias plays an important role in the dependence of galaxy properties on environments.

In such a comparison between different clusters at different redshifts, we must keep in mind that the size and mass of the clusters can be different. In fact, the bolometric X-ray luminosity of 1716 cluster is  $\sim 3$  times larger than that of 2215 cluster (Ettori et al. 2004; Stanford et al. 2006). Also, the sub-structures of 1716 cluster is more prominent (Koyama et al. 2007). We cannot therefore conclude whether the difference seen in spatial distribution is largely due to time evolution or due to different masses or characteristics. But it may be the case that we are witnessing the evolution in star forming activity in the core of high- $z$  clusters from  $z \sim 1.5$  to  $z \sim 0.8$ .

On the other hand, Finn et al. (2005) report a diversity in distribution of  $H\alpha$  emitters in the cores of clusters at  $z=0.7-0.8$ . Two among their three clusters at similar redshifts show a decrease in  $H\alpha$  fraction toward the cluster centre, while the other cluster shows an opposite trend. This fact may imply that it is not only the star formation bias that causes the high fraction of [O II] emitters in the core of the 2215 cluster. It is thus crucial to observe more clusters at  $z > 1.0$ , and to evaluate to what extent the presence of star forming galaxies in the cluster core is a general property at  $z > 1$ .

The  $L_X - T$  relation of the 2215 cluster suggests that it is possible that it experienced a merger event within the last few Gyr (Hilton et al. 2007). This can be another possible reason for the high fraction of [O II] emitters, since the cluster merging event might cause an enhancement of star formation activity in galaxies in the cluster core. Also, since the distribution of [O II] emitters is projected on celestial sphere, it may be possible that some member galaxies in

the outskirts of the cluster happen to be seen in the direction to the cluster centre, which may result in apparent high fraction of [O II] emitters at the centre. However, the number density of galaxies in the outskirts is likely to be much lower than that of galaxies in the core region (Figure 3(b)), and such projection effect would be small in the direction to the centre.

It is also possible that an active galactic nucleus (AGN) enhances [O II] line flux. Recent studies suggest that a fraction of AGNs in clusters increases with redshifts. Galametz et al. (2009) have found an overdensity of AGNs within a radius of 0.25 Mpc in clusters at  $z > 0.5$ , and that the density of X-ray selected AGNs in clusters at  $1.0 < z < 1.5$  is  $0.102 \text{ arcmin}^{-2}$ , which is  $\sim 2$  times larger than that of clusters at  $0.5 < z < 1.0$ . It indicates that it is possible that 3–4 AGNs reside in the central  $33.8 \text{ arcmin}^2$  region of the 2215 cluster. Martini, Sivakoff & Mulchaey (2009) also show a monotonous increase of AGN fraction in clusters from  $z \sim 0.2$  to  $z \sim 1.0$ . It is worth mentioning that Stanford et al. (2006) report no obvious X-ray point source in the cluster core, although we cannot completely exclude the presence of any point source. We thus consider that AGN contribution is small. Yan et al. (2006) suggest that [O II] emitters in the red sequence tend to be AGNs, most commonly LINERs, and that [O II] line can be valid as an indicator of star formation activity only for blue galaxies. We find four red [O II] emitters with  $z' - K_s$  colours redder than  $-0.088K_s + 4.26$  (see §4.3 and Figure 9(a)), which are located near the centre (Figure 5). Even if all these red [O II] emitters are AGNs, the enhancement of galaxy activity in the core would be still valid, since the presence of AGN is also a sign of activity. This would then provide us with the clues to understanding the influence of AGNs on the evolution of massive galaxies in the cluster core, such as quenching of star formation. It is essential therefore to obtain NIR spectra of these four [O II] emitters in order to constrain the origin of the [O II] lines.



## 4.2 SFR, specific SFR and equivalent width

According to Ly et al. (2007), [O II] line flux [ergs s<sup>-1</sup> cm<sup>-2</sup>] and continuum flux density [ergs s<sup>-1</sup> cm<sup>-2</sup> Å<sup>-1</sup>] for 44 [O II] emitters are calculated from flux densities in NB912 and z' bands ( $f_{NB912}$  and  $f_{z'}$ ), respectively, as follows;

$$F([\text{O II}]) = f_{NB912} \Delta_{NB912} \frac{1 - (f_{z'}/f_{NB912})}{1 - (\Delta_{NB912}/\Delta_{z'})}, \quad (3)$$

$$f_{\lambda, \text{cont}} = f_{z'} \frac{1 - (f_{NB912}/f_{z'}) (\Delta_{NB912}/\Delta_{z'})}{1 - (\Delta_{NB912}/\Delta_{z'})}, \quad (4)$$

where  $\Delta_{NB912}$  and  $\Delta_{z'}$  indicate FWHMs of the filters, and  $\Delta_{NB912} = 134\text{\AA}$  and  $\Delta_{z'} = 955\text{\AA}$ .

In order to estimate dust-corrected SFR of our [O II] emitters, we use the empirical SFR calibration for [O II] parametrized in terms of the *B*-band luminosity developed by Moustakas, Kennicutt & Tremonti (2006) for local star forming galaxies. The *B*-band luminosity was regarded as a proxy of stellar mass. They were aware that the mass-to-light ratios of star forming galaxies span a wide range and that the *B*-band luminosity would not be a perfect indicator of stellar mass. However, they empirically found that the amount of dust extinction and metallicity are correlated with the *B*-band luminosity (see Figure 16 in Moustakas et al. (2006)). They also found that the correlation for star forming galaxies at  $0.5 < z < 1.5$  is roughly consistent with that for local galaxies. It should be noted, however, that there is a larger uncertainty in the derived SFR for individual galaxies at high redshifts. We apply their correction scheme of dust extinction to our [O II] emitters at  $z = 1.46$ . We infer the rest-frame *B*-band fluxes from the *J*-band fluxes and  $z - J$  colours and use them to correct for dust extinction. Figure 8(a) shows thus derived dust-corrected SFRs of our [O II] emitters as a function of distance from the cluster center.

Stellar masses of the [O II] emitters are estimated from  $K_s$  total magnitudes using the equation given in Daddi et al. (2004). Daddi et al. (2004) estimate the stellar masses for *K*-selected galaxies at  $z > 1.4$  using K20 survey data. Mass to *K*-band luminosity ratio is derived from multi-wavelength data from *U* to *K* with Salpeter (1955) IMF (Fontana et al. 2004). The relation is calibrated with  $z - K$  colour, which can reduce the dispersion of derived stellar mass to  $\sigma(\Delta \log(M_*)) = 0.20$ . We also derive specific SFR by dividing SFR by stellar mass. Figure 8(b) shows the specific SFRs for [O II] emitters as a function of radius from a centre.

The observed equivalent width of an [O II] emission is also derived from [O II] line flux and continuum flux density (Equations (3) and (4)). Figure 8(c) shows the observed equivalent widths for the [O II] emitters as a function of radius from a centre.

Figure 8 suggests that star formation activities of the [O II] emitters in denser regions are as active as those in the outskirts of the cluster. The equivalent widths are not correlated with the position of galaxies in the cluster. These facts also suggest active star formation in the central region of the 2215 cluster. On the other hand, the specific SFRs may show a mild correlation in the sense that [O II] emitters at the inner regions tend to have lower specific SFRs. Since the similar correlation is not seen in their SFRs, this is due to the fact that massive galaxies tend to reside near

the centre of the cluster. This tendency may be due to the galaxy formation bias that massive galaxies are formed in the cluster core, or may be a result of efficient mass assembly due to merging that can be more effective in high density regions. Figure 8(b) also shows that the red [O II] emitters tend to have lower specific SFRs. This may be because we underestimate their intrinsic SFRs due to the strong dust extinction for the red galaxies. Otherwise, this may imply that these galaxies are just quenching their star formation activities.

## 4.3 Colour-magnitude diagram

Figure 9(a) shows a colour-magnitude diagram of  $z' - K_s$  vs.  $K_s$  for cluster member candidates in the central  $2' \times 2'$  region. Note that the  $K_s$ -selected galaxy sample is used in this section. The use of the NB912-selected sample may cause incompleteness in the number of galaxies at faint  $z'$  magnitudes. The solid line in the figure shows the expected location of the colour-magnitude relation (CMR) of passively evolving galaxies at  $z = 1.46$  formed at  $z_{form} = 5$  inferred from the Kodama et al. (1998) model which is calibrated to reproduce the CMR of elliptical galaxies in the Coma cluster at  $z = 0$ ;

$$z' - K_s = -0.088K_s + 4.56. \quad (5)$$

We define the red sequence galaxies as those falling in-between  $\Delta(z' - K_s) = \pm 0.3$  from the predicted CMR as shown by the broken lines in Figure 9(a).

The number of the red sequence galaxies seems to decrease at magnitude fainter than  $K_s \sim 21.5$ . The long-dashed and dotted lines show the  $5\sigma$  and  $3\sigma$  confidence levels of  $z' - K_s$  colours, respectively. Therefore the decrease in the number of the red galaxies is not driven by incompleteness. Stanford et al. (2006) and Hilton et al. (2009) also examine colour-magnitude diagrams, and find that there is a well defined CMR of red galaxies in the 2215 cluster. In Stanford et al. (2006), however, shallowness of the data does not allow us to discuss the faint end of the red sequence. Hilton et al. (2009) use deeper data to investigate the CMR, and colour-magnitude diagram of Figure 6 in Hilton et al. (2009) shows a deficit of red galaxies at magnitudes fainter than  $K_s \sim 21.5$ . This is consistent with our result.

Since all the cluster member candidates are plotted in Figure 9(a), some galaxies actually do not belong to the cluster. In order to correctly evaluate the deficit of the red galaxies, we derive the field-corrected  $K_s$ -band luminosity function in the central  $2' \times 2'$  region by statistically subtracting the field contamination. The detection completeness is also corrected for as follows. Artificial objects with Gaussian profile are randomly generated and embedded in the raw  $K_s$  image, and detection of these objects is conducted with the same manner as in §3.1. The assumed distribution of brightness of the artificial objects is uniform within each magnitude bin. The completeness thus estimated in each bin is always as high as  $\gtrsim 90\%$ .

The resulting luminosity function of the red sequence galaxies is shown in Figure 9(b). It is clear that the number of red member galaxies decreases at  $K_s \lesssim 21.5$ . This magnitude corresponds to  $K_s^* + 0.5$  with respect to the passively evolving galaxies at  $z = 1.46$  (Kodama et al. 1998). In the

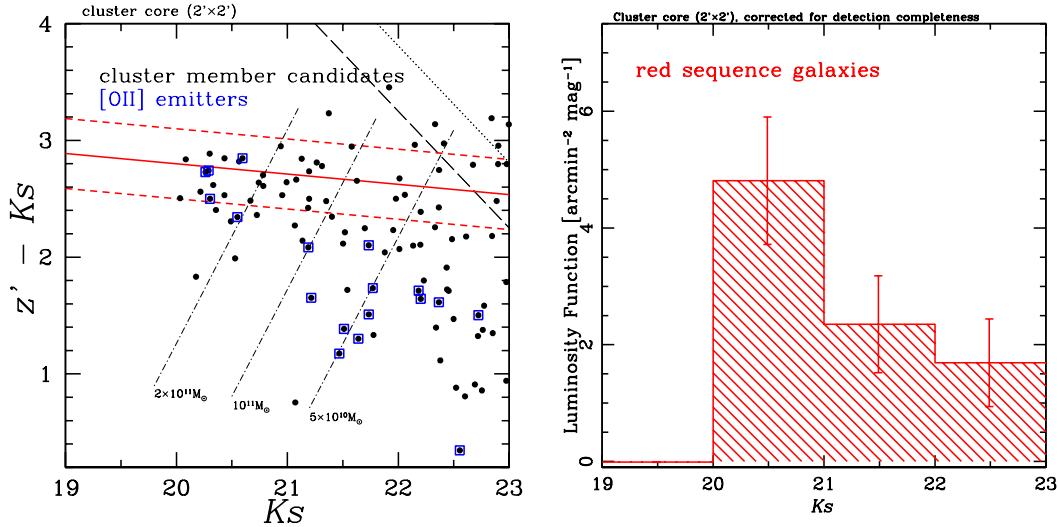


**Figure 9.** (a) Left panel: Colour-magnitude diagram of  $z' - K_s$  vs.  $K_s$  for the  $K_s$ -detected galaxies in the central  $2' \times 2'$  region. Black dots shows cluster member candidates. Red solid line show the expected location of the colour-magnitude relation of passively galaxies at  $z = 1.46$  formed at  $z_{form}=5$  (Kodama et al. 1998). We define the red sequence galaxies as those falling between the two broken lines,  $\Delta(z' - K_s) = \pm 0.3$  around the colour-magnitude relation. Long-dashed and dotted lines are  $3\sigma$  and  $5\sigma$  confidence levels in colours, respectively. Blue open squares show 18 [O II] emitters in this region. Three dot-dashed lines indicate iso-stellar mass curves for  $2 \times 10^{11} M_\odot$ ,  $10^{11} M_\odot$  and  $5 \times 10^{10} M_\odot$ , respectively, which are drawn based on the equation given in Daddi et al. (2004). (b) Right panel:  $K_s$ -band luminosity function of the red sequence galaxies in the central  $2' \times 2'$  region. The contribution of field galaxies, estimated from the SDF sample, is statistically subtracted. Error-bars show Poisson errors.

2215 cluster at  $z = 1.46$ , the red sequence is visible only down to  $\sim K_s^* + 0.5$  and truncated at that magnitude.

Such truncation is seen, if any, at fainter magnitudes ( $\gtrsim M^* + 0.5$ ) in the cores of lower redshift clusters. For example, Andreon (2006) find no deficit of galaxies on red sequence down to  $M^* + 3.5$  in the MS1054.4-0321 cluster at  $z=0.83$ . Koyama et al. (2007) suggest that the build-up of the CMR depends on X-ray luminosity of clusters at  $z \sim 0.8$ , and find that the CMR is established down to  $M^* + 2.0$  even for a X-ray fainter cluster RXJ1716+6708 at  $z = 0.81$ . Lidman et al. (2004) and Tanaka et al. (2008) study CMR for the RDCS J1252.9-2927 cluster at  $z=1.24$ . While the red sequence galaxies only appear down to  $K \sim 22$  in sub-clumps in the outskirts of the cluster (Tanaka et al. 2008), faint red galaxies clearly exist down to  $K \sim 24$  in the main cluster (Lidman et al. 2004). Lidman et al. (2008) also find that there are red faint galaxies down to  $K \sim 24.5$  in the core region of the XMMU J2235.3-2557 cluster at  $z=1.39$ . We also note that Kodama et al. (2007) show that the CMR of proto-clusters at much higher redshifts ( $2 \lesssim z \lesssim 3$ ) becomes less conspicuous, and even the bright-end of the red sequence seems to disappear in proto-clusters at  $z \gtrsim 2.5$ .

In Figure 9(a), we mark the [O II] emitters with blue open squares. Most of the [O II] emitters have bluer colours as expected since they are likely to be still forming stars. The galaxies that are fainter in  $K_s$  hence less massive galaxies tend to be slightly bluer. This may suggest that star formation activity in more massive galaxies tends to be truncated at earlier times. We draw three iso-stellar mass curves of  $2 \times 10^{11} M_\odot$ ,  $10^{11} M_\odot$  and  $5 \times 10^{10} M_\odot$ , respectively, using the equation given in Daddi et al. (2004). If the [O II] emitters cease their star formation, they would move along these curves until they reach on to the red sequence. If an [O II] emitter has a SFR of  $50 M_\odot/\text{yr}$ , which is close to the

median SFR in our [O II] emitter sample, and keeps this rate constant until  $z = 1.0$ , its stellar mass would increase by  $\Delta M_s \simeq 7 \times 10^{10} M_\odot$ . If we assume that an [O II] emitter gradually becomes red while increasing its stellar mass at a constant SFR, the faint end of the red sequence would be filled up by  $z \sim 1.0$ . If this is the case, the [O II] emitters with  $\lesssim 5 \times 10^{10} M_\odot$  may be good progenitors of the faint galaxies on the red sequence. However, we do not know yet the mechanisms of changing galaxy colours and quenching their star formation. As described in the last paragraph of §4.1, contribution of AGNs to the [O II] emitters on the red sequence can be large (Yan et al. 2006). Perhaps AGN feedback is one of the key mechanisms to reduce the star formation activities.

Combining with the previous studies of CMR (see above), we come up with the following scenario of formation of red sequence in clusters at  $z \sim 1.5$ . The most massive galaxies brighter than  $K_s^*$  (i.e.,  $> 10^{11} M_\odot$ ) are formed at  $z > 2$ , and become red by quenching the star formation in early epoch. Some galaxies on the red sequence may still be keeping residual star formation activities. On the other hand, less massive galaxies are actively growing at  $z < 2$ , and we hardly see galaxies fainter than  $K_s^*$  on the red sequence. Star forming galaxies with  $\sim 5 \times 10^{10} M_\odot$  at  $z \sim 1.5$  may evolve into faint red sequence galaxies by  $z \sim 1.0$ . This suggest down-sizing propagation of star formation in high redshift clusters.

## 5 SUMMARY

We performed a unique, unbiased [O II] line survey of star forming galaxies in the XMMXCS J2215.9-1738 cluster at

$z = 1.46$ , which is currently the most distant cluster ever identified with a detection of extended X-ray emission.

We have obtained wide-field optical ( $B$ ,  $z'$ ,  $NB912$ ) and near-infrared ( $J$  and  $K_s$ ) data with Suprime-Cam and MOIRCS, respectively. With a combination of  $NB912$  narrow-band filter ( $\lambda_c = 9139\text{\AA}$ ,  $\text{FWHM}=134\text{\AA}$ ) and the  $z'$ -band filter, we detect 69  $NB912$  emitters in the central  $6' \times 6'$  region where near-infrared data are also available. Among them, 44 emitters are identified as [O II] emitters associated to the cluster based on the  $B - z'$  and  $z' - K_s$  colours, down to a dust-free star formation rate of  $2.6 \text{ M}_\odot \text{ yr}^{-1}$  ( $3\sigma$ ).

We find that many [O II] emitters reside in the central high density region even within a radius of 0.25 Mpc (physical scale). We also find that the fraction of [O II] emitters to cluster members remains high up to the core region. This suggests that the 2215 cluster is still actively forming stars even at the central region, in contrast to lower redshift clusters, where old passively evolving elliptical galaxies dominate. This indicates an inside-out propagation of star formation in high redshift clusters, and we may be eventually beginning to enter the epoch of biased galaxy formation in the densest region at  $z = 1.46$ .

SFRs, specific SFRs, and equivalent widths are derived for 44 [O II] emitters. It is found that the emitters have similar SFRs and equivalent widths irrespective of the location within the cluster. It seems however that the specific SFRs tend to decrease slightly toward the cluster core, probably due to the fact that more massive [O II] emitters exist near the centre. We may be approaching to the formation phase of massive galaxies at the cluster core.

Moreover, the colour-magnitude diagram in the 2215 cluster shows a deficit of red sequence galaxies fainter than  $\sim M^* + 0.5$ , while the red sequence in lower redshift clusters extends to much fainter magnitudes. While some bright [O II] emitters are located on the red sequence, all the faint [O II] emitters with  $> M^*$  have blue colours. It is likely that those blue [O II] emitters become redder once they truncate their star formation, and they would eventually reach and fill the faint end of the red sequence at lower redshifts. This indicates a down-sizing propagation of star formation in high redshift clusters.

## ACKNOWLEDGMENTS

The optical and near-infrared data used in this paper are collected at the Subaru Telescope, which is operated by the National Astronomical Observatory of Japan. We thank the Subaru Telescope staff for their invaluable help to assist our observations with Suprime-Cam and MOIRCS. We are grateful to Dr. Masayuki Tanaka for carefully reading the manuscript, and for his valuable comments. We thank Dr. Chun Ly for kindly providing us with the NB921 emitter catalogue in the Subaru Deep Field. We also thank Dr. Masafumi Yagi for providing us with some data reduction codes for the optical imaging data, and for instruction of the reduction procedures. We would like to thank an anonymous referee for useful comments and suggestions. M.H. and Y.K. acknowledges support from the Japan Society for the Promotion of Science (JSPS) through JSPS Research Fellowship for Young Scientists. This work was financially supported in part by the Grant-in-Aid for Scientific Research

(Nos. 18684004 and 21340045) by the Japanese Ministry of Education, Culture, Sports, and Science.

## REFERENCES

- Abadi M. G., Moore B. & Bower R. G., 1999, MNRAS, 300, 947  
 Andreon S., 2006, MNRAS, 369, 969  
 Bertin E. & Arnouts S., 1996, A&AS, 117, 393  
 Butcher H., & Oemler A. Jr., 1978, ApJ, 219, 18  
 Butcher H., & Oemler A. Jr., 1984, ApJ, 285, 426  
 Cardelli J. A., Clayton G. C., & Mathis J. S., 1989, ApJ, 345, 245  
 Cen R., & Ostriker J. P., 1993, ApJ, 417, 415  
 Coleman G. D., Wu C.-C., & Weedman D. W., 1980, ApJS, 43, 393  
 Cooper M. C., Newman J. A., Croton D. J. et al., 2006, MNRAS, 370, 198  
 Cooper M. C., Newman J. A., Weiner B. J. et al., 2008, MNRAS, 383, 1058  
 Cowie L. L., Songaila A., Hu E. M., & Cohen J. G., 1996, AJ, 112, 839  
 Daddi E., Cimatti A., Renzini A., Fontana A., Mignoli M., Pozzetti L., Tozzi P., & Zamorani G., 2004, ApJ, 617, 746  
 Dressler A., Oemler A. Jr., Couch W. J. et al., 1997, ApJ, 490, 577  
 Ellingson E., Lin H., Yee H. K. C., & Carlberg R. G., 2001, ApJ, 547, 609  
 Elbaz D., Daddi E., Le Browner D. et al., 2007, A&A, 468, 33  
 Ettori S., Tozzi P., Borgani S., & Posati P., 2004, A&A, 417, 13  
 Finn R. A., Zaritsky D., McCarthy D. W. Jr. et al., 2005, ApJ, 630, 206  
 Fontana A., Pozzetti L., Donnarumma I. et al., 2004, A&A, 424, 23  
 Galametz A., Stern D., Eisenhardt P. R. M. et al., 2009, ApJ, 694, 1309  
 Gunn J. E., & Stryker, L. L., 1983, ApJS, 52, 121  
 Hayashi M., Shimasaku K., Motohara K., Yoshida M., Okamura S., & Kashikawa N., 2007, ApJ, 660, 72  
 Hilton M., Collins C. A., Stanford S. A. et al., 2007, ApJ, 670, 1000  
 Hilton M., Stanford S. A., Stott J. P. et al., 2009, ApJ, 697, 436  
 Ichikawa T., Suzuki R., Tokoku C. et al., 2006, Proc. SPIE, 6269, 38  
 Ideue Y., Nagao T., Taniguchi Y. et al., 2009, ApJ, 700, 971  
 Kamata Y., Miyazaki S., Nakaya H. et al., 2008, Proc. SPIE, 7021, 52  
 Kennicutt R. C., 1998, ARA&A, 36, 189  
 Kodama T., Arimoto N., Barger A. J., & Aragón-Salamanca A., 1998, A&A, 334, 99  
 Kodama T., & Bower R. G., 2001, MNRAS, 321, 18  
 Kodama T., Yamada T., Akiyama M. et al., 2004a, MNRAS, 350, 1005  
 Kodama T., Balogh M. L., Smail I., Bower R. G., & Nakata F., 2004b, MNRAS, 354, 1103  
 Kodama T., Tanaka I., Kajisawa M., Kurk J., Venemans

- B., de Breuck C., Vernet J., & Lidman C., 2007, MNRAS, 377, 1717
- Kong X., Daddi E., Arimoto N. et al., 2006, ApJ, 638, 72
- Koyama Y., Kodama T., Tanaka M., Shimasaku K., & Okamura S., 2007, MNRAS, 382, 1719
- Koyama Y., Kodama T., Shimasaku, K. et al., 2008, MNRAS, 391, 1758
- Koyama, Y. et al., 2010, MNRAS, submitted
- Landolt A. U., 1992, AJ, 104, 340
- Leggett S. K., 2006, MNRAS, 373, 781
- Lidman C., Rosati P., Demarco R., Nonino M., Mainieri V., Stanford S. A., & Toft S., 2004, A&A, 416, 829
- Lidman C., Rosati P., Tanaka M. et al., 2008, A&A, 489, 981
- Ly C., Malkan M. A., Kashikawa N. et al., 2007, ApJ, 657, 738
- Margoniner V. E., de Carvalho R. R., Gal R. R., & Djorgovski S. G., 2001, ApJ, 548, 143
- Martini P., Sivakoff G. R., & Mulchaey J. S., 2009, ApJ, 701, 66
- Miyazaki S., Komiyama Y., Sekiguchi M. et al., 2002, PASJ, 54, 833
- Motohara K., Hayashi M., Shimasaku K., Yoshida M., Kashikawa N., & Kodama T., 2008, ASPC, 399, 274
- Moustakas J., Kennicutt R. C. J., & Tremonti C. A., 2006, ApJ, 642, 775
- Nakata F., Bower R. G., Balogh M. L., & Wilman D. J., 2005, MNRAS, 357, 679
- Oke J. B., 1990, AJ, 99, 1621
- Ouchi M., Shimasaku K., Okamura S. et al., 2004, ApJ, 611, 660
- Poggianti B. M., Desai V., Finn R. et al., 2008, ApJ, 684, 888
- Postman M., Lubin L. M., & Oke J. B., 2001, AJ, 122, 1125
- Quilis V., Moore B., & Bower R., 2000, Sci, 288, 1617
- Salpeter E. E., 1955, ApJ, 121, 161
- Schlegel D. J., Finkbeiner D. P. & Davis M., 1998, ApJ, 500, 525
- Stanford S. A., Romer A. K., Sabirli K. et al., 2006, ApJ, 646, L13
- Suzuki R., Tokoku C., Ichikawa T. et al., 2008, PASJ, 60, 1347
- Tanaka M., Kodama T., Arimoto N., Okamura S., Umetsu K., Shimasaku K., Tanaka I., Yamada T., 2005, MNRAS, 362, 268
- Tanaka M., Finoguenov A., Kodama T. et al., 2008, A&A, 489, 571
- Tasca L. A. M., Kneib J. P., Iovino A. et al., 2009, A&A, 503, 379
- Yagi M., Kashikawa N., Sekiguchi M., Doi M., Yasuda N., Shimasaku K., & Okamura S., 2002, AJ, 123, 66
- Yan R., Newman J. A., Faber S. M., Konidaris N., Koo D., & Davis M., 2006, ApJ, 648, 281